CHIN. PHYS. LETT. Vol. 37, No. 4 (2020) 047801 **Express Letter**

High-Pressure Ultrafast Dynamics in Sr_2IrO_4: Pressure-Induced Phonon Bottleneck Effect *

Yanling Wu(吴艳玲)[1†], Xia Yin(尹霞)[2†], Jiazila Hasaien(加孜拉·哈赛恩)[1,3], Yang Ding(丁阳)[2**], Jimin Zhao(赵继民)[1,3,4**]

[1]*Beijing National Laboratory for Condensed Matter Physics, Institute of Physics, Chinese Academy of Sciences, Beijing 100190*

[2]*Center for High-Pressure Sciences and Technology Advanced Research, Beijing 100094*

[3]*School of Physical Sciences, University of Chinese Academy of Sciences, Beijing 100049*

[4]*Songshan Lake Materials Laboratory, Dongguan 523808*

(Received 13 February 2020)

By integrating pump-probe ultrafast spectroscopy with diamond anvil cell (DAC) technique, we demonstrate a time-resolved ultrafast dynamics study on non-equilibrium quasiparticle (QP) states in Sr_2IrO_4 under high pressure. On-site in situ condition is realized, where both the sample and DAC have fixed position during the experiment. The QP dynamics exhibits a salient pressure-induced phonon bottleneck feature at 20 GPa, which corresponds to a gap shrinkage in the electronic structure. A structural transition is also observed at 32 GPa. In addition, the slowest relaxation component reveals possible heat diffusion or pressure-controlled local spin fluctuation associated with the gap shrinkage. Our work enables precise pressure dependence investigations of ultrafast dynamics, paving the way for reliable studies of high-pressure excited state physics.

PACS: 78.47.J−, 78.47.jg, 62.50.−p, 71.38.−k DOI: 10.1088/0256-307X/37/4/047801

Ultrafast dynamics investigation of non-equilibrium excited states of quantum materials has witnessed great triumph in uncovering the mysteries behind various interactions,[1−7] complex phase transitions,[3,7] as well as bosonic collective excitations.[2−4,7−9] However, to date, ultrafast pump-probe spectroscopy has mainly been applied to investigate quantum states under ambient pressure, leaving the high pressure dynamics physics largely unexplored. High-pressure means has been employed to directly modify the lattice parameters, thus to tune the electronic states, leading to the discovery of novel phenomena in superconducting,[10,11] topological,[12,13] correlated,[14] thermoelectric,[15] and other systems. However, so far, none of these discoveries are within the excited state regime. The above-Fermi-surface physics is barely explored in the realm of high pressure physics. Here we report a successful synthesis of the two fields together. We realize a reliable ultrafast pump-probe dynamics investigation under high pressure, by which we discover a pressure-induced phonon bottleneck effect that is not reported before.

Combining high pressure study with ultrafast dynamics investigation is both intriguing and promising for the advancement of condensed matter physics. For example, recently the combination between NV center technique and DAC has attracted great interest in the community.[16−19] Because a pump-probe experiment needs spatial overlap of the pump and probe beams, it is more crucial to maintain the sample position absolutely unchanged in the light path during the tuning and calibration of the high pressure. So far, although there have been a few reports on ultrafast dynamics investigations at high pressure,[20−22] there are no explicit reports or discussions on a truly reliable *in situ* pump-probe experiment (*i.e.*, no explicit report on whether the DACs remained fixed in the light path during the experiments, especially when tuning and calibrating the pressure). Here we present a successful *on-site in situ* ultrafast spectroscopy study on a correlated 5*d* material iridate Sr_2IrO_4 at high pressure, which greatly enhances the reliability of exploring the high-pressure ultrafast dynamics science.

Single-layer iridate Sr_2IrO_4 belongs to the Ruddlesden–Popper family ($Sr_{n+1}Ir_nO_{3n+1}$, $n = 1$, 2, and ∞) and has been theoretically predicted for possible realization of novel superconductivity.[23] Moreover, its strong spin–orbit coupling (SOC) causes its isotropic SU(2) symmetry to break, which results in strong interplays among all the charge, spin, orbital, and lattice degrees of freedom.[23,24] A number of high-pressure studies on Sr_2IrO_4 have been reported.[25−27] Ultrafast dynamics investigations have also been carried out.[7,28] However, to our limited knowledge, there has been no report on high-pressure ultrafast dynamics investigation on Sr_2IrO_4 or any other iridates.

In this work, we successfully design and implement an *on-site in situ* ultrafast pump-probe spectroscopy

*Supported by the National Key Research and Development Program of China (Grant Nos. 2017YFA0303603, 2016YFA0300303, 2018YFA0305703), the National Natural Science Foundation of China (Grant Nos. 11774408, 11574383, 11874075, U1530402), the Strategic Priority Research Program of CAS (Grant No. XDB30000000), the International Partnership Program of Chinese Academy of Sciences (Grant Nos. GJHZ1826, GJHZ1403), the Beijing Natural Science Foundation (Grant No. 4191003), the Science Challenge Project (Grant No. TZ2016001), and the CAS Interdisciplinary Innovation Team.

†These authors contributed equally to this work.

**Corresponding authors. Email: jmzhao@iphy.ac.cn; yang.ding@hpstar.ac.cn

under high pressure. We find a high-pressure-induced phonon bottleneck effect, which is not known before in condensed matter physics. A pressure-induced gap shrinkage at 20 GPa is also evidenced. Our slowest relaxation data reveal possible heat diffusion or pressure-tuned local residual spin fluctuation, and we also observe a structural transition occurring at 32 GPa. Our results contribute to the excited state ultrafast dynamics investigation at high pressure, which advances the synthesis of the two fields.

We design and implement an *on-site in situ* collinear microscopic ultrafast pump-probe spectroscopy setup, whereby the sample is hosted in a high-pressure DAC. The schematic experimental setup is depicted in Fig. 1.[3,29] We use a regenerative Ti:sapphire amplifier to deliver ultrafast pulses of 800 nm central wavelength, 80 fs pulse duration, and 250 kHz repetition rate. The incident ultrashort laser pulses are split into pump and probe beams. We employ a collinear scheme, where an objective lens is used to focus both the pump and probe beams onto the sample surface with normal incidence. After the sample, the reflected probe beam traverses through the same objective lens. To reduce interference, the pump beam is frequency-doubled by a BBO crystal to yield 400 nm pulses. The 3.1 eV photons are absorbed by the valence electrons in Sr_2IrO_4, leading to interband transitions, where the excited states are probed by the concomitant 800 nm probe pulses. The single crystal is anchored in a DAC with a diameter of 300 microns, which is compressed gradually to 44.5 GPa with a gas membrane control system.

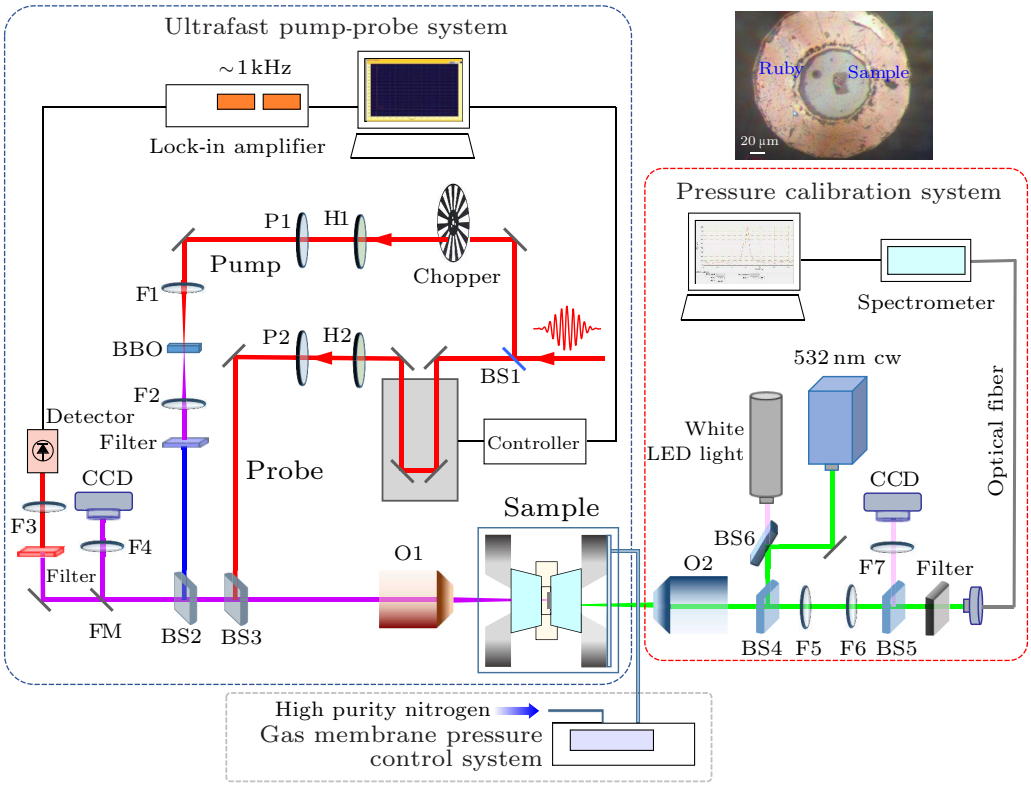

Fig. 1. Schematic experimental setup for the *on-site in situ* time-resolved ultrafast spectroscopy at high pressure. The system composes three parts: the ultrafast pump-probe system, the pressure control system, and the pressure calibration system. Collinear microscopy pump-probe system, gas membrane system, and back surface *in situ* calibration system are employed. Right top panel: photograph of the sample. BS: beam splitter; H: half wavelength plate; P: Polarizer; F: focusing lens; BBO: nonlinear crystal; FM: flip mirror; O: objective lens.

We define "*on-site in situ*" as that the DAC (with sample) is not taken out of the light path during the experiment, including tuning and calibrating pressure. The advantage is that no sample motion or rotation is introduced during the experiment; hence the maximum reliability can be achieved by excluding sample surface spot-to-spot fluctuation and ensuring spatial overlap of pump and probe beams. To realize the *on-site in situ* experiment, we arrange the DAC in a transmission geometry and employ a gas membrane control system, where the pressure calibration is carried out from the back direction of the DACs (Fig. 1).

We detect the reflection of the probe beam by using a lock-in technique to enhance the signal-to-noise ratio. Cross polarization geometry is also implemented to further enhance the signal-to-noise ratio. The diameters ($1/e^2$ beam diameter) of the pump and probe beams are 4.8 μm and 6.7 μm, respectively. The pump and probe fluences are kept at 2.66 mJ/cm^2 and 0.45 mJ/cm^2, respectively, which are set to minimize the thermal effects from laser heating (our 250 kHz system is helpful in reducing the integrated thermal

effect, as compared with the 80 MHz systems). In the upper-right panel of Fig. 1, we show a microscope photograph of a typical Sr_2IrO_4 single crystal (in dimensions of $20 \times 40\,\mu m^2$; for details of sample preparation, see Text A in the Supplementary Materials) loaded in a DAC.

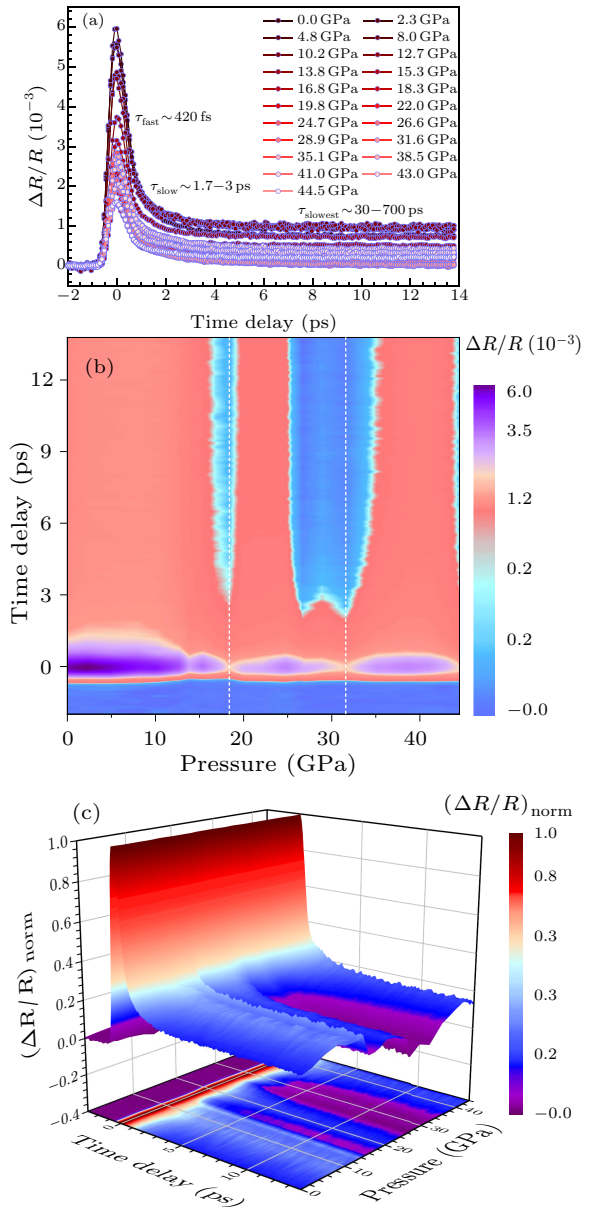

Fig. 2. High-pressure ultrafast dynamics of Sr_2IrO_4. (a) Relative differential reflectivity $\Delta R/R$ at different pressures. (b) Color map of the pressure-dependent $\Delta R/R$ shown in (a). White lines: guide to the eyes. (c) Normalized $\Delta R/R$ as a function of pressure. In both (b) and (c) the color contrast regions reveal changes in excited sate dynamics.

In Fig. 2(a) we show our main result of the time-resolved photo-induced transient differential reflectivity ($\Delta R/R$) of Sr_2IrO_4 over a range from 0.0 GPa to 44.5 GPa at room temperature. Upon the pump pulse excitation, the ground-state carriers in the equilibrium state are excited nearly instantaneously to the excited state, resulting in a rapid positive peak of $\Delta R/R$ at the so-called time zero ($t = 0$ ps). The value of $\Delta R/R$ is proportional to the density of photo-induced excited state free carriers, which varies with the delay time between the probe and pump pulses. The initial ultrafast relaxation component (within ~ 1 ps) exhibits a relatively short lifetime, which is in line with the known small gap (in the order of 0.1 eV) insulating phase of Sr_2IrO_4 at room temperature.[30] The ultrafast QP dynamics varies prominently with increasing pressure, in both the amplitudes and lifetimes. Note that the pressure dependence of the reflectivity R exhibits no features (see Text B and Fig. S1 in the Supplementary Materials), which excludes possible pressure-induced changes in reflectivity itself and potential contaminations from the diamonds.

To investigate the effects of pressure through excited state carrier dynamics, we map out the $\Delta R/R$ values as functions of time and pressure in Fig. 2(b). Qualitatively, two special color regions show up: one is the 16.5–19 GPa region (blue region centered at 18 GPa), the other is the 25–35 GPa region (blue region centered at 31.5 GPa). Two white dashed lines separate the three purple zones, reflecting the changes in the ultrafast dynamics and making possible pressure effects.

Figure 2(c) is a 3D color map of the normalized $\Delta R/R$ to highlight the pressure-dependent QP dynamics in more details. The initial relaxation right after the pump excitation is quite similar for all pressure, as they all exhibit nearly identical color after the time zero in the map. This indicates that the fast component, which reflects the electron-phonon interaction,[3,4] is nearly immune to compression. The relatively slow component(s) are more complicated, showing clear pressure dependence. Two purple color regions (16.5–19 GPa and 25–35 GPa) mark their different dynamics.

We further quantitatively analyze the data in Fig. 2. Analysis of each scanning trace shows that the relaxation process can be decomposed into three components (see Text C and Fig. S2 in the Supplementary Materials), namely the fast, slow, and slowest decaying components. The time-resolved pump-probe data can be fitted by $\Delta R/R = A_{fast}\ \exp(-t/\tau_{fast}) + A_{slow}\ \exp(-t/\tau_{slow}) + A_{slowest}\ \exp(-t/\tau_{slowest})$, where A_{fast}, A_{slow}, and $A_{slowest}$ are the amplitudes, τ_{fast}, τ_{slow} and $\tau_{slowest}$ are the lifetimes. A typical data fitting result is shown in Fig. S2, where the inset explicitly presents a long-range scanning trace up to 160 ps, with a slowest relaxation lifetime of about 240 ps.

The fitting results of the pressure-dependent amplitudes and lifetimes are summarized in Fig. 3. The fast decay component (Figs. 3(a) and 3(b)) reflects the electron-phonon scattering.[31,32] With increasing pressure, A_{fast} decreases gradually and then more rapidly at $P < 18$ GPa, till reaching the minimum at ~ 20 GPa. Passing 20 GPa, A_{fast} increases and then decreases, till exhibiting a minimum at 32 GPa (Fig. 3(a)). The τ_{fast} is nearly a constant (0.42 ps) for

the whole pressure range (Fig. 3(b)), indicating a constant electron-phonon coupling strength for the whole pressure range.

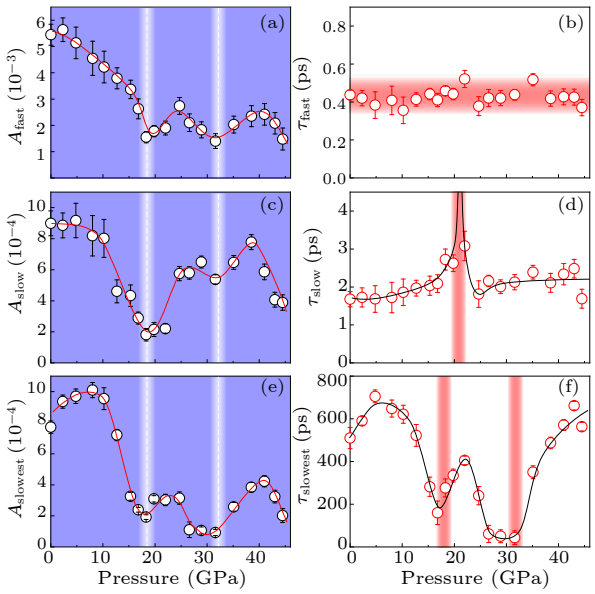

Fig. 3. Pressure-induced phonon bottleneck effect and gap shrinkage. Pressure dependence of the (a) amplitude A_{fast} and (b) lifetime τ_{fast} of the fast component relaxation, where the red bar in (b) marks the unchanged lifetime. (c)–(d) Pressure dependence of the slow component, where the red bar marks a salient enhancement of lifetime τ_{slow} at 20 GPa and the red curve exhibits a pronounced decrease in A_{slow} before 20 GPa. (e)–(f) Pressure dependence of the slowest component dynamics. The red and black curves are guides to the eyes. The white bars in (a), (c), (e) denote the two pressure-induced physical effects evidenced in QP dynamics.

The slow decay component (Figs. 3(c) and 3(d)) reflects the phonon decay.[31,32] The A_{slow} is initially constant, then drops quickly, and eventually reaches a minimum also at 18–20 GPa. For $P > 20$ GPa, A_{slow} exhibits a variation tendency similar to that of A_{fast} (Fig. 3(c)). Significantly, τ_{slow} exhibits a distinct quasi-divergence behavior at $P = 20$ GPa (Fig. 3(d)). It increases starting from a lower pressure, continuously increases till reaching a maximum value at $\sim$ 20 GPa, and then decreases abruptly to a constant value for $P > 25$ GPa. The simultaneous observation of both prominent decrease in A_{slow} and salient enhancement trend in τ_{slow} at 18–20 GPa clearly demonstrates a pressure-induced phonon bottleneck effect,[3–5,33–35] which has not been reported before. Note that an amplitude fitting curve extension is usually needed in determining the critical point (see Fig. 2(c) of Ref. [36]). Phonon bottleneck effect has been well established for decades, initially mainly concerning spin-lattice scatterings with relatively long lifetimes detectable by using microwaves and oscilloscopes.[37] With the advent of ultrafast spectroscopy, phonon bottleneck resulting from faster electron-phonon scatterings can be detected,[33] especially has been frequently observed in strongly correlated materials.[5,6,36,3] The excited state QPs and phonons are in a microscopic quasi-equilibrium, which only breaks up when all the high frequency phonons (which has an energy large enough to promote the carriers to above the gap) diminish (through either decaying into lower energy elementary excitations or propagating away from the active region). When a gap shrinks with temperature (or, as shown here, with pressure), more phonons act as "high frequency phonons". As a result, the QPs can hardly relax to the ground state, leading to an elongated lifetime—a token of phonon bottleneck, if simultaneously with amplitude decrease.

The phonon bottleneck effect we observe indicates a gap shrinkage with increasing pressure at 20 GPa, which to some extent suggests the inauguration of a quasi-phase-transition.[3,5,33] The gap shrinks sharply at 20 GPa, and becomes a small constant at $P > 20$ GPa. This is very similar to the closing of a superconducting gap,[3,5,33] except that here temperature is replaced by pressure and no Cooper pairing gets involved in. The shrinkage of the insulating gap is understandable, because pressure normally broadens the bandwidth of the electronic structure, thus increasing the conductivity. It is reported that the resistance experiences a sharp reduction when approaching 18 GPa, reaching a lowest nearly constant value at around 20 GPa near room temperature.[25,26] It is also reported that the gap shrinks from 60 meV at ambient pressure to 30 meV at 20 GPa at 50–100 K (the gap will be even smaller at room temperature).[25]

The slowest decay component (Figs. 3(e) and 3(f)) may be attributed to various possible origins. The lifetime $\tau_{slowest}$ varies within 30–700 ps, which is roughly in line with (A) heat diffusion process, which usually occurs in 100 ps–1 ns[35] or (B) spin-lattice scattering, which usually occurs in 20 ps–1 ns.[31,38,39] For a few reasons, we cannot conclude (A) is unambiguously the mechanism: the 30 ps lifetime we observe is not perfectly in concert with such a scenario; we use a 250 kHz setup, which generates relatively smaller thermal heating; taking 11.2 GPa as an example, we observe straight linear relations in Fig. 4, which indicates no fluence saturation; and we do not observe a constant A_0 in the data analysis. Alternatively, scenario (B) cannot be ruled out as the underling mechanism. The spin-lattice scattering process occurs at a timescale of tens to hundreds of ps,[31,38,39] and should be distinguished from those relaxations involving spins but without lattice. The latter occurs at a much shorter timescale (<10 ps) and often relies on long-range magnetic ordering,[28] which is not true for our case at room temperature. Scenario (B) requires the existence of spins in the sample. It has been reported that, for Sr_2IrO_4, residual local spin fluctuations still survive at $T > T_N = 240$ K.[40,41] Thus, with increasing pressure, the local residual spin fluctuation remains and is strongly modified by pressure. Consequently, we attribute the slowest component to either (A) or (B) and leave its verification to future investiga-

tions. By tuning high pressure, $A_{\rm slowest}$ has a similar variation trend as those of $A_{\rm fast}$ and $A_{\rm slow}$, which indicates that at 20 GPa multiple degrees of freedom are coupled together. We furthermore assign the variation at 32 GPa to a structural phase transition.[25,27,42]

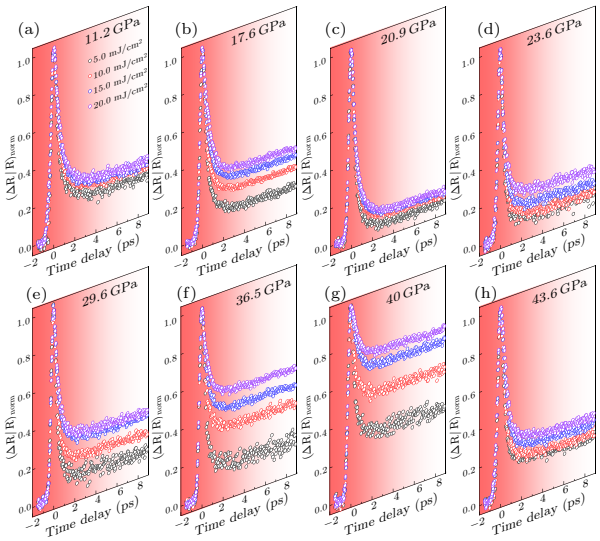

Fig. 4. Normalized fluence dependence of ultrafast dynamics at different pressures. The dynamics, especially the lifetimes, are similar (a), (c), (d), (h) or notably different at some pressure regions (b), (e)–(g).

Finally, we investigate the fluence-dependence of the ultrafast dynamics under different pressures. The normalized data are shown in Fig. 4. The excited state QPs exhibit different fluence-dependent ultrafast relaxations. While the overall fluence dependences are close to each other (exhibiting similar lifetimes, see Figs. 4(a), 4(c), 4(d), and 4(h)), they appear prominently different (exhibiting different lifetimes, see Figs. 4(b), 4(e)-4(g)) at nearby 18 GPa and within the 29.6–40 GPa region. The change in the fluence dependence must have an intrinsic origin, which is affected by the external pressure. To explicitly illustrate this, we plot the amplitudes and lifetimes of the three components in Fig. 5, with their fluence dependences, where the data are offset for clarity. We use color-filled solid symbols to represent the out-of-linear-relation components, leaving those of regular linear-relation denoted by vacant symbols. Saturation occurs in two pressure ranges: the 17.6–20.9 GPa range (red and blue curves) and the 36.5–40.0 GPa range (brown and purple curves).

For the 17.6–20.9 GPa region, $A_{\rm fast}$, $A_{\rm slow}$, and $A_{\rm slowest}$ all exhibit nonlinear fluence dependences, manifesting the complex effect of gap shrinkage on the carrier generation. For the 36.5–40.0 GPa region, $A_{\rm fast}$, $A_{\rm slow}$, and $A_{\rm slowest}$ again all exhibit nonlinear fluence dependences, manifesting the effect of the structural phase transition occurring at 32 GPa. For the lifetimes, $\tau_{\rm fast}$ exhibits nonlinear dependences in the 17.6–20.9 GPa and 36.5–40.0 GPa regions, which are caused by the effect of gap shrinkage and structural phase transition, respectively. The $\tau_{\rm slow}$ and $\tau_{\rm slowest}$ are nearly constants, indicating that the phonon-phonon scattering, as well as spin-scattering, is not affected by the fluence. For high pressure investigations the sample size is relatively small, making thermal effect a more crucial challenge for high pressure ultrafast optical spectroscopy. Observing the linear fluence-dependence of amplitudes and lifetimes (Fig. 5) thus demonstrates that we have successfully avoided the thermal effect.

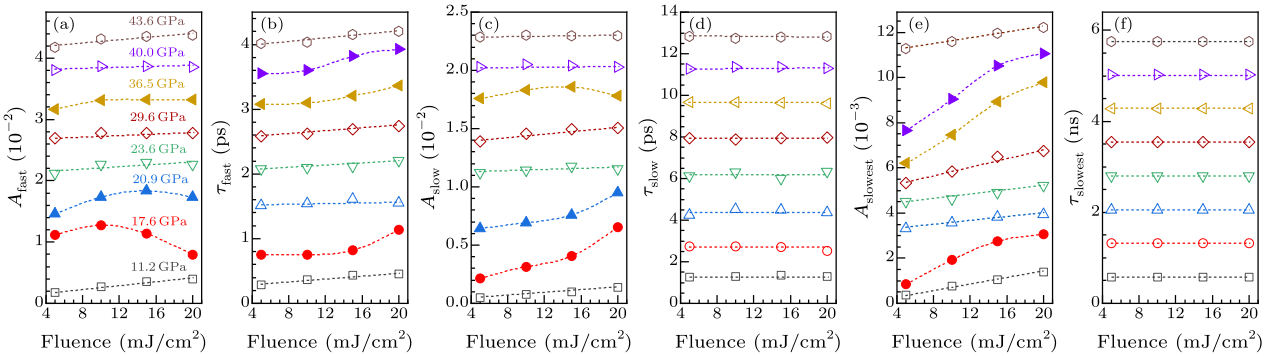

Fig. 5. Effect of pressure on the laser fluence dependence of the ultrafast dynamics. (a)–(b) Fluence dependence of the fast component. (c)–(d) Fluence dependence of the slow component. (e)–(f) Fluence dependence of the slowest component. Data are offset for clarity. The solid symbols mark nonlinear dependences, and the vacant symbols represent linear dependences.

In summary, we have demonstrated a reliable experimental design combining the ultrafast spectroscopy with the high-pressure experiment. We have successfully realized *on-site in situ* ultrafast dynamics investigation under high pressure. Significantly, we find a pressure-induced phonon bottleneck effect in Sr_2IrO_4, which is new to condensed matter physics. Moreover, our data reveal the existence of pressure-induced gap shrinkage at room temperature. We also observe features consistent with a structural phase transition at 32 GPa and possible pressure-controlled local spin-lattice scattering. Our investigation paves

the way for high pressure ultrafast dynamics science, enabling the exploration of vast quantum materials and novel states in a previously untouched realm.

References

[1] Orenstein J 2012 *Phys. Today* **65** 44
[2] Zhao J M, Bragas A V, Lockwood D J and Merlin R 2004 *Phys. Rev. Lett.* **93** 107203
[3] Tian Y C, Zhang W H, Li F S, Wu Y L, Wu Q, Sun F, Zhou G Y, Wang L L, Ma X C, Xue Q K and Zhao J M 2016 *Phys. Rev. Lett.* **116** 107001
[4] Wu Q, Zhou H X, Wu Y L, Hu L L, Ni S N, Tian Y C, Sun F, Zhou F, Dong X L, Zhao Z X and Zhao J M 2019 arXiv:1910.09859 [cond-mat.supr-con]
[5] Demsar J, Podobnik B, Kabanov V V, Wolf T and Mihailovic D 1999 *Phys. Rev. Lett.* **82** 4918
[6] Hsieh D, Mahmood F, Torchinsky D H, Cao G and Gedik N 2012 *Phys. Rev. B* **86** 035128
[7] Matsunaga R, Tsuji N, Fujita H, Sugioka A, Makise K, Uzawa Y, Terai H, Wang Z, Aoki H and Shimano R 2014 *Science* **345** 1145
[8] Sun F, Wu Q, Wu Y L, Zhao H, Yi C J, Tian Y C, Liu H W, Shi Y G, Ding H, Dai X, Richard P and Zhao J M 2017 *Phys. Rev. B* **95** 235108
[9] Hu L L, Yang M, Wu Y L, Wu Q, Zhao H, Sun F, Wang W, He R, He S L, Zhang H, Huang R J, Li L F, Shi Y G and Zhao J M 2019 *Phys. Rev. B* **99** 094307
[10] Guo J, Zhou Y Z, Huang C, Cai S, Sheng Y T, Gu G D, Yang C L, Lin G C, Yang K, Li A G, Wu Q, Xiang T and Sun L L 2020 *Nat. Phys.* **16** 295
[11] Medvedev S, McQueen T M, Troyan I A, Palasyuk T, Eremets M I, Cava R J, Naghavi S, Casper F, Ksenofontov V, Wortmann G and Felser C 2009 *Nat. Mater.* **8** 630
[12] Kirshenbaum K, Syers P S, Hope A P, Butch N P, Jeffries J R, Weir S T, Hamlin J J, Maple M B, Vohra Y K and Paglione J 2013 *Phys. Rev. Lett.* **111** 087001
[13] Bahramy M S, Yang B J, Arita R and Nagaosa N 2012 *Nat. Commun.* **3** 679
[14] Sun J P, Jiao Y Y, Yi C J, Dissanayake S E, Matsuda M, Uwatoko Y, Shi Y G, Li Y Q, Fang Z and Cheng J G 2019 *Phys. Rev. Lett.* **123** 047201
[15] Ravichandran N K and Broido D 2019 *Nat. Commun.* **10** 827
[16] Shang Y X, Hong F, Dai J H, Yu H, Lu Y N, Liu E K, Yu X H, Liu G Q and Pan X Y 2019 *Chin. Phys. Lett.* **36** 086201
[17] Hsieh S, Bhattacharyya P, Zu C, Mittiga T, Smart T J, Machado F, Kobrin B, Höhn T O, Rui N Z, Kamrani M, Chatterjee S, Choi S, Zaletel M, Struzhkin V V, Moore J E, Levitas V I, Jeanloz R and Yao N Y 2019 *Science* **366** 1349
[18] Yip K Y, Ho K O, Yu K Y, Chen Y, Zhang W, Kasahara S, Mizukami Y, Shibauchi T, Matsuda Y, Goh S K and Yang S 2019 *Science* **366** 1355
[19] Lesik M, Plisson T, Toraille L, Renaud J, Occelli F, Schmidt M, Salord O, Delobbe A, Debuisschert T, Rondin L, Loubeyre P and Roch J F 2019 *Science* **366** 1359
[20] Kasami M, Mishina T and Nakahara J 2004 *Phys. Status Solidi B* **241** 3113
[21] Trigo M, Chen J, Jiang M P, Mao W L, Riggs S C, Shapiro M C, Fisher I R and Reis D A 2012 *Phys. Rev. B* **85** 081102(R)
[22] Cantaluppi1 A, Buzzi M, Jotzu G, Nicoletti D, Mitrano M, Pontiroli D, Riccò M, Perucchi A, Pietro P D and Cavalleri A 2018 *Nat. Phys.* **14** 837
[23] Cao G and Schlottmann P 2018 *Rep. Prog. Phys.* **81** 042502
[24] Torchinsky D H, Chu H, Zhao L, Perkins N B, Sizyuk Y, Qi T, Cao G and Hsieh D 2015 *Phys. Rev. Lett.* **114** 096404
[25] Haskel D, Fabbris G, Zhernenkov M, Kong P P, Jin C Q, Cao G and van Veenendaal M 2012 *Phys. Rev. Lett.* **109** 027204
[26] Zocco D A, Hamlin J J, White B D, Kim B J, Jeffries J R, Weir S T, Vohra Y K, Allen J W and Maple M B 2014 *J. Phys.: Condens. Matter* **26** 255603
[27] Samanta K, Ardito F M, Souza-Neto N M and Granado E 2018 *Phys. Rev. B* **98** 094101
[28] Afanasiev D, Gatilova A, Groenendijk D J, Ivanov B A, Gibert M, Gariglio S, Mentink J, Li J, Dasari N, Eckstein M, Rasing T, Caviglia A D and Kimel A V 2019 *Phys. Rev. X* **9** 021020
[29] Zhao J M, Bragas A V, Merlin R and Lockwood D J 2006 *Phys. Rev. B* **73** 184434
[30] Ge M, Qi T F, Korneta O B, De Long D E, Schlottmann P, Crummett W P and Cao G 2011 *Phys. Rev. B* **84** 100402(R)
[31] Kirilyuk A, Kimel A V and Rasing T 2010 *Rev. Mod. Phys.* **82** 2731
[32] Perfetti L, Loukakos P A, Lisowski M, Bovensiepen U, Wolf M, Berger H, Biermann S and Georges A 2008 *New J. Phys.* **10** 053019
[33] Rothwarf A and Taylor B N 1967 *Phys. Rev. Lett.* **19** 27
[34] Kabanov V V, Demsar J and Mihailovic D 2005 *Phys. Rev. Lett.* **95** 147002
[35] Giannetti C, Capone M, Fausti D, Fabrizio M, Parmigiani F and Mihailovic D 2016 *Adv. Phys.* **65** 58
[36] Kabanov V V, Demsar J, Podobnik B and Mihailovic D 1999 *Phys. Rev. B* **59** 1497
[37] Anderson P W 1959 *Phys. Rev.* **114** 1002
[38] Ogasawara T, Ohgushi K, Tomioka Y, Takahashi K S, Okamoto H, Kawasaki M and Tokura Y 2005 *Phys. Rev. Lett.* **94** 087202
[39] Chia E E M, Talbayev D, Zhu J X, Yuan H Q, Park T, Thompson J D, Panagopoulos C, Chen G F, Luo J L, Wang N L and Taylor A J 2010 *Phys. Rev. Lett.* **104** 027003
[40] Fujiyama S, Ohsum H, Komesu T, Matsuno J, Kim B J, Takata M, Arima T and Takagi H 2012 *Phys. Rev. Lett.* **108** 247212
[41] Ishii K, Jarrige I, Yoshida M, Ikeuchi K, Mizuki J, Ohashi K, Takayama T, Matsuno J and Takagi H 2011 *Phys. Rev. B* **83** 115121
[42] Zhang J B, Yan D Y, Yesudhas S, Deng H S, Xiao H, Chen B J, Sereika R, Yin X, Yi C J, Shi Y G, Liu Z X, Pärschke E M, Chen C C, Chang J, Ding Y and Mao H K 2019 *npj Quantum Mater.* **4** 23

Supplementary Materials: High-pressure ultrafast dynamics in Sr_2IrO_4: pressure-induced phonon bottleneck effect*

Yanling Wu (吴艳玲)[1†], Xia Yin (尹霞)[2†], Jiazila Hasaien (加孜拉 哈赛恩)[1,3], Yang Ding (丁阳)[2]**, Jimin Zhao (赵继民)[1,3,4]**

[1] *Beijing National Laboratory for Condensed Matter Physics, Institute of Physics, Chinese Academy of Sciences, Beijing 100190, China*

[2] *Center for High-Pressure Sciences and Technology Advanced Research, Beijing 100094, People's Republic of China*

[3] *School of Physical Sciences, University of Chinese Academy of Sciences, Beijing 100049, China*

[4] *Songshan Lake Materials Laboratory, Dongguan, Guangdong 523808, China*

** *Corresponding author. Jimin Zhao, Email: jmzhao@iphy.ac.cn; Yang Ding, Email: yang.ding@hpstar.ac.cn.*

† *These authors contributed equally.*

Text A: Sample preparation

High-purity source materials $SrCO_3$, IrO_2 and $SrCl_2\ 6H_2O$ powders were mixed together and placed in a platinum crucible, the materials have a molar ratio of 4:1:20. The crucible was heated until the temperature reached 1478 K and stayed for about 9 hours, then slowly cooled until it reached room temperature. After standing for 3 hours, the synthetic product was separated and washed with deionized water to obtain high-purity single crystals. The single crystals have typical dimensions $0.8 \times 0.8 \times 0.3$ mm^3. The lattice structure of Sr_2IrO_4 is in the tetragonal phase (space group is $I4_1/acd$) at ambient pressure.

Text B: Pressure-dependence of the reflectivity R

When we measure the differential reflectivity ΔR for each given pressure value, we also measure R itself. The results are summarized in Fig. S1. It can be seen the pressure dependence does not exhibit prominent features at 20 GPa and 32 GPa. This indicates that we do not observe possible contaminations from the diamonds, which otherwise may potentially mix with our signal ΔR/R in Fig. 2.

Text C: Data fitting with three exponential decays

We explicitly demonstrate the analysis for our data. Figure S2 shows a typical scanning trace of the relative differential reflectivity ΔR/R (at 24.7 GPa). We fit the data with the sum of three exponential decay functions (red solid curve). The three individual exponential components are marked by blue, yellow, and purple dashed curves, respectively. The red curve is the sum of the three components, which overall fits our data very well. The inset shows its long-range scanning data, which corresponds to a $\tau_{slowest}$ of 240 ps. The time domain data shown in the inset also clearly demonstrates that the third component is an exponential decay rather than a constant value.

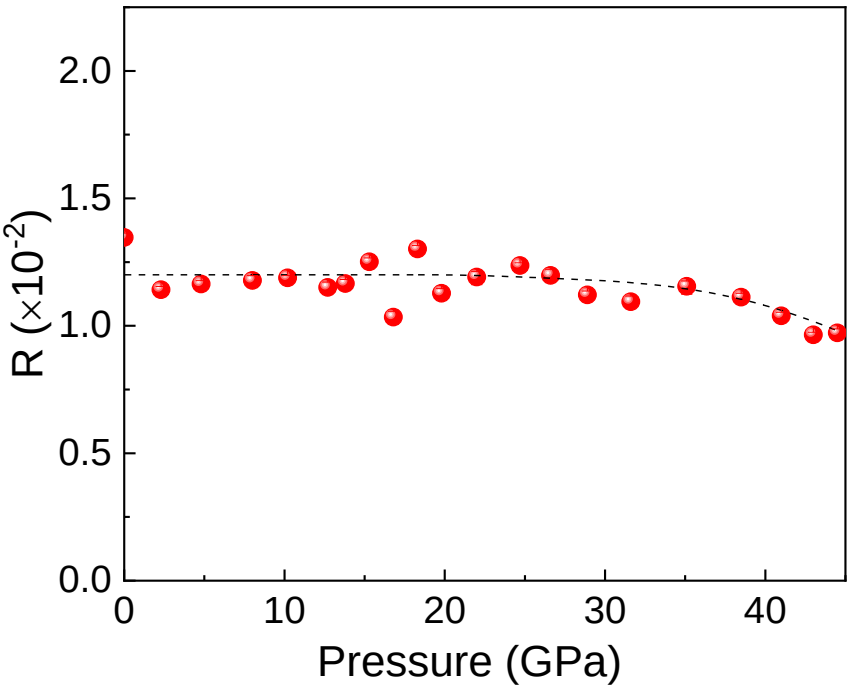

Fig. S1: Pressure dependence of the probe beam reflectivity R. The red dots are reflectivity values R taken at each given pressure, respectively, when measuring the corresponding differential reflectivity ΔR. The dashed curve is a guide to the eyes showing no feature at 20 and 32 GPa.

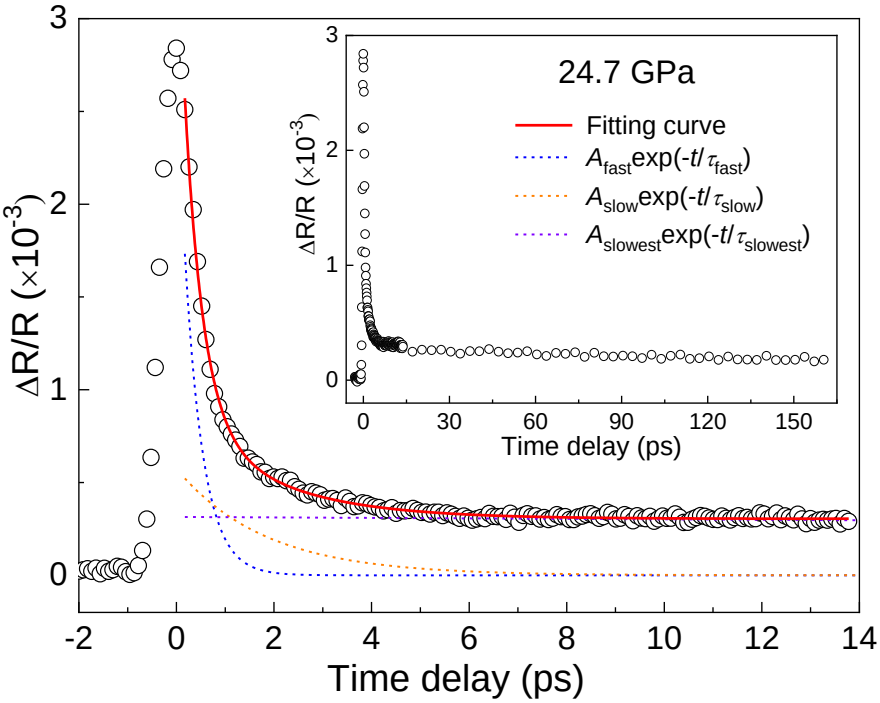

Fig. S2: Data analysis of ΔR/R for a typical scanning trace. The red solid curve is the fitting result, which is a sum of the three exponential decay functions, depicted by the dashed yellow, blue, and purple curves, respectively. Inset: Temporal zoom-out view showing the long scanning range ultrafast dynamics.